Mechanistic Modeling of CO_2 Well Leakage in a Generic Abandoned Well Through a Bridge Plug Cement-Casing Gap

L. Pan and C.M. Oldenburg

Energy Geosciences Division

Lawrence Berkeley National Laboratory

Berkeley, CA 94720

February 20, 2020

Keywords: Mechanistic modeling; CO_2 and brine leakage; bridge plug failure; abandoned well

Note that this is the manuscript form of the near-final version of the paper. Please read and cite the final published paper:

Pan, L. and Oldenburg, C.M., 2020. Mechanistic modeling of CO2 well leakage in a generic abandoned well through a bridge plug cement-casing gap. *International Journal of Greenhouse Gas Control*, *97*, p.103025.

Abstract

Both known and unmapped plugged and abandoned wells are potential leakage pathways for CO_2 from geologic carbon sequestration (GCS) sites. Although many abandoned wells have cement bridge plugs installed to prevent leakage, the seal between the cement and the inner casing wall is subject to failure. In this study, we carried out detailed T2Well simulations of cases of sudden non-Darcy flow of CO_2 and brine leakage up the gap between a cement plug and the inner steel casing wall that becomes a fully connected flow path during the post-injection period. The goal of our study was two-fold: (1) to understand the dynamics, rates, and the characteristic temporal signals associated with the onset of leakage through various gap-aperture sizes, and (2) to suggest potential monitoring strategies based on the findings. Simulation results show that the leakage of CO_2 and brine upward is transient with interesting phase interference behavior. Time-dependent oscillatory flows with varying pressure, temperature, and flow rates of CO_2 and brine show strong dependence on gap aperture. Phase-change and decompression lead to very low temperatures at the top of the well for gap apertures larger than 4 mm suggesting that remote thermal monitoring at the ground surface may be an effective way of monitoring even if well locations are not known a priori. Pressure in the well is also indicative of CO_2 leakage. The temporal patterns of changing temperature and pressure may be useful diagnostic signals for leakage detection. Finally, these transient leakage signals may provide information on the cause of leakage and/or characteristics of the flow path that could inform effective remediation design and execution approaches.

Introduction

Both known and unknown (unmapped) plugged and abandoned wells are widely recognized as potential pathways for CO_2 and brine to leak from geologic carbon sequestration (GCS) sites into potable groundwater aquifers and even back into the atmosphere (Gasda et al., 2004). Wells are often abandoned by a procedure involving emplacement of a cement bridge plug at depth, above which the well is filled with fluids such as brine, drilling mud, or corrosion-inhibiting fluid. The purpose of the cement bridge plug is to seal off the well from the reservoir, hydraulic communication to which is provided by perforations. The purpose of the fluid above the bridge plug is to maintain pressure and prevent rapid corrosion of the steel casing. Experience has shown that cement-casing interfaces are subject to debonding and other processes over time that lead to failure to seal that creates a leakage flow path for formation fluids and CO_2 upward past the plug into the fluid-filled well.

Before a plugged and abandoned well that is leaking up its inner casing string to the surface or into shallow soils above a buried well top can be fixed, the leakage must be detected and stopped. Challenges arise because CO_2 leakage rates through degraded cement seals may be small and fluid leakage manifestations on the ground surface from plugged and abandoned wells may be difficult to detect within natural background variations of moisture and CO_2 concentration. In this study,

we have carried out detailed non-Darcy flow simulations of the transient period following the onset of CO_2 and brine leakage up the gap in a bridge plug between cement and inner casing wall and into the open fluid-filled column of a prototypical abandoned well. We vary the plug gap aperture and simulate two different bridge-plug lengths (10 m and 30 m) to investigate sensitivity of leakage signals to plug-gap properties. One purpose of this study is to provide information on expected leakage behavior dynamics and the temporal signals associated with non-isothermal CO_2 and brine leakage that can be used to design near-surface monitoring approaches for leakage detection. Through mechanistic modeling of viscous two-phase flow in the well-reservoir system, the reasons for various interesting dynamic behaviors can be explained. The simulation approach is general enough that the plug gap can also be conceived as being a fracture in the cement bridge plug with axial length equal to the plug thickness and horizontal length equal to one-half of the plug perimeter.

Background and Prior Work

Integrity failures in pre-existing wells of all kinds (abandoned, idled, shut-in, operating) completed to reservoir depth within the footprint of the CO_2 free-phase and/or pressure plumes of GCS sites are widely recognized as a potential cause of CO_2 and brine leakage from future large-scale GCS operations. There are several components of wells and critical interface seals that can fail over time and allow leakage to occur as summarized by Gasda et al. (2004). Of the several well integrity failure modes, failures resulting in open gaps and annuli, e.g., between cement and casing or between cement and formation, are considered by researchers studying CO_2 and brine leakage in the GCS context to be most likely to result in large leakage flow (Kutchko et al., 2007; Bachu and Bennion, 2009). Laboratory and field studies in the GCS context have found that chemical reactions between cement and carbonic acid (CO_2 dissolved in water) can degrade cement integrity (net dissolution) and in other cases lead to precipitation and self-sealing of gaps and spaces (Carey et al., 2007; Crow et al., 2007). Nevertheless, the large number of documented cases of sustained casing pressure (SCP) in oil and gas wells (Bourgoyne et al., 1999; Choi et al., 2013; Lackey et al., 2017) suggests that gaps and annuli are generally present in wells (Huerta et al., 2009). At least one example exists in the GCS context of poor bonding of cement to steel casing that can lead to gaps and annular spaces that compromise well integrity (e.g., Oldenburg et al., 2011).

Given the general concern for the integrity of existing wells, a large body of work exists focusing on the evaluation of the leakage rates and total leakage that could occur as a result of well integrity failure, along with remediation approaches (e.g., Wojtanowicz et al., 2001). Early studies were aimed at evaluating and mitigating sustained casing pressure (SCP) in oil and gas wells (e.g., Xu and Wojtanowicz, 2001), and these methods were further developed more recently (Huerta et al., 2009; Tao et al., 2010). As interest in GCS grew in the early 2000's, new semi-analytical approaches to modeling well leakage related to CO_2 and brine were developed and applied (e.g., Nordbotten et al., 2004; 2005). In addition, numerical methods including consideration of two-phase flow were developed and applied (e.g., Pruess, 2003; Celia et al., 2005; Ebigbo et al., 2007).

Reduced order models (ROMs) for well leakage and aquifer impact have been developed by the U.S. Department of Energy's National Risk Assessment Partnership (NRAP) for quantification of the uncertainty of estimated leakage impacts (Pawar et al., 2016). Despite the large number of studies and solution approaches, all of the prior well leakage models except for NRAP's open-well leakage ROM (Pan and Oldenburg, 2016) have assumed that well leakage flow was through an effective porous medium, i.e., by the process of Darcy flow. While this assumption may be adequate for many cases involving SCP and/or low-flow-rate or incipient leakage through fine cracks or through tortuous paths in degraded cement, CO_2 and brine leakage through finite-aperture gaps and annuli between cement and casing should formally be modeled as viscous flow rather than Darcy flow.

In the study presented here, we simulate the onset and transient period of well leakage by single-, two-, and three-phase viscous (non-Darcy) flow in gaps or annuli of various apertures along a cement plug at the cement-casing interface within an idealized abandoned well. The conceptual model we assume is that the cement plug was sealing the abandoned well effectively up until some time during the post-injection period of the GCS project when the gap became fully connected across the plug and the well started to leak. Leakage along such a gap leads to reservoir fluid (CO_2 and/or brine) entering the fluid-filled column above the plug where non-Darcy pipe flow occurs by pressure gradient or buoyancy forces. At certain conditions, two types of CO_2-rich phases can exist, namely, gaseous CO_2 and liquid CO_2, which can lead to a three-phase (aqueous, gaseous CO_2 and liquid CO_2) system at different depths in the well. In all cases, we simulate the entire coupled reservoir-well (plug gap and well column) system upward to the top of the well at the ground surface considering coupled reservoir flow (Darcy flow) and open gap and column flow (non-Darcy flow). As it will be shown, these gap-leakage flow processes occur over time scales much smaller than expected chemical reaction time scales which were not included in our model. In order to focus on the flow processes and transient leakage signals, we also neglect for now geomechanical processes. To our knowledge, this is the first study that simulates the mechanistic non-isothermal process of three-phase flow in a narrow gap related to CO_2 and brine well leakage from a hypothetical GCS reservoir.

Conceptual Model

The prototypical abandoned well system that we simulate is shown in Fig. 1. In the system, a 1989 m-long column of inhibitor fluid (assumed to be pure water in this study) fills an open well above a 10 m-long cement bridge plug with an open gap (e.g., due to debonding) over part of its circumference (50%). Although the current U.S. regulations require longer cement plugs for abandoned wells (e.g., extending 100 ft above oil bearing strata), many older wells abandoned prior to the 1950s either were not plugged at all or were plugged with very little cement in them (NPC, 2011). The requirement on length of cement plug is rather vague prior to the 1970s in the U.S. The longer the cement plug is, the lower the chance to be subject to through-going gaps and the greater the resistance is to leakage flow if a gap were to develop. We use a 10 m-long cement

plug to reflect poor plugs in those older wells that are more vulnerable to leakage without losing the general features of leakage through a failed plug in abandoned wells. Additional results for a 30 m-long plug are presented for comparison.

The perforated bottom section of the well is in hydraulic connection with the permeable CO_2-filled reservoir. As with many plugged and abandoned wells, there is no wellhead and the top of the casing is conceptualized as being covered by a permeable rusted steel plate and 1 m of soil (Fig. 1a), both of which we model as porous media coupled to the open well. The thickness of the semi-circular gap between the cement plug and the casing wall is varied as a parameter in the simulations. Reservoir fluids (CO_2 and brine) have the potential to leak up the gap between the cement of the bridge plug and the inner casing wall into the column of inhibitor fluid and onward to the ground surface through the permeable materials (rusted steel plate and soil) at the top of the well. Note that although this is a coupled well-reservoir model, we do not intend to simulate the full development process of the CO_2-filled reservoir. Instead, we investigate possible dynamic behaviors of leakage when plug failure takes place in an abandoned well connected to a CO_2-filled reservoir during the post-injection period of the GCS reservoir.

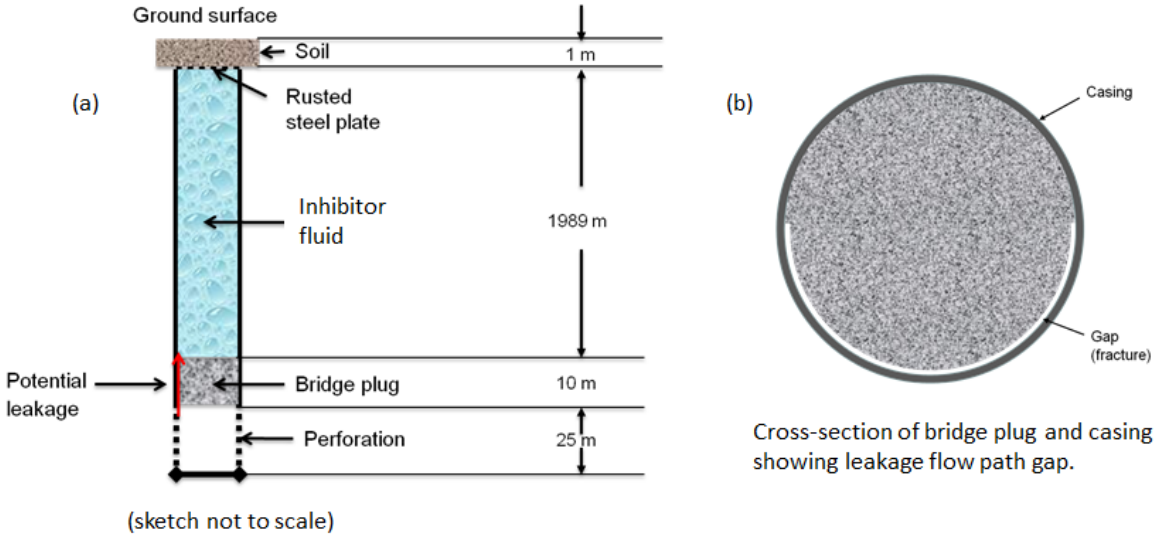

Figure 1. (a) Conceptual model of prototypical abandoned well with bridge plug below long open section, and (b) cross section of bridge plug showing the gap (over one-half of the circumference) the aperture of which was varied in the simulations shown here. The reservoir and other formations (cap rock, soil etc.) are included in the model (see Figure 2 and related text for details of the integrated well-reservoir model used in this study).

The properties of the modeled system for the 10 m-long plug are presented in Tables 1 and 2. We note that all of the layers in the model (Table 2) are assumed to have pore compressibility of 3×10^{-9} Pa^{-1}, and that all layers have thermal conductivities of 3.0 W/(m ºC) and specific heats of 1000 J/(kg ºC).

Table 1. Well and plug properties.

Feature	Value
Well length	2024 m (from -1 m to -2025 m)
Casing ID	0.15962 m (7-inch casing, wall thickness = 9.09 mm)
Bridge plug	10 m thickness (from -1990 to -2000 m)
Perforation	25 m (from -2000 m to -2025 m)
Wall roughness of well	45×10^{-6} m
Wall roughness of plug gap	100×10^{-6} m
Gap aperture	Various
Effective porosity	Various, a function of aperture
Effective perimeter of gas	Various, a function of aperture
Rusted steel plate at top of the abandoned well	Assumed same permeability as cover soil (100 Darcy)

Table 2. Layer properties.

Layer	Depth (m)	Porosity	Lateral permeability (m^2)	Vertical permeability (m^2)
Reservoir sand	2000-2025	0.25	10^{-12}	10^{-12}
Cap rock	1980-2000	0.05	10^{-18}	10^{-18}
Overburden	10-1980	0.05	10^{-18}	10^{-18}
Soil2	1-10	0.45	10^{-15}	10^{-15}
Soil1	0-1	0.45	10^{-10}	10^{-10}

All formation layers above the reservoir are saturated with water under hydrostatic pressure. The bottom formation layer is modeled (with 25 grid layers) to represent a GCS reservoir with a given initial gas (CO_2-rich phase) saturation (0.5 in this study) and initial pressure at the bottom grid cell equal to the hydrostatic pressure. Because of the existence of gas phase, the initial pressure at the top of the reservoir is slightly (1 bar) larger than the hydrostatic pressure that would exist at the same depth (1986 m below land surface) if the reservoir were fully saturated with water. The wellbore above the reservoir (including the plug) is initially saturated with water under hydrostatic pressure whereas the wellbore below the plug is under the same conditions as the reservoir. The geothermal gradient is 30 ^{o}C/km and the ambient temperature at land surface is assumed to be 25 ^{o}C. The entire domain is under natural ambient thermal conditions initially. Conditions at the top of the model are held at atmospheric pressure and ambient temperature (25 ^{o}C). In all cases we use a radially symmetric (*RZ*) grid with variable radial and vertical grid spacing (Fig. 2). a no-flow boundary is assigned along the lateral boundary at 1000 m away from the well.

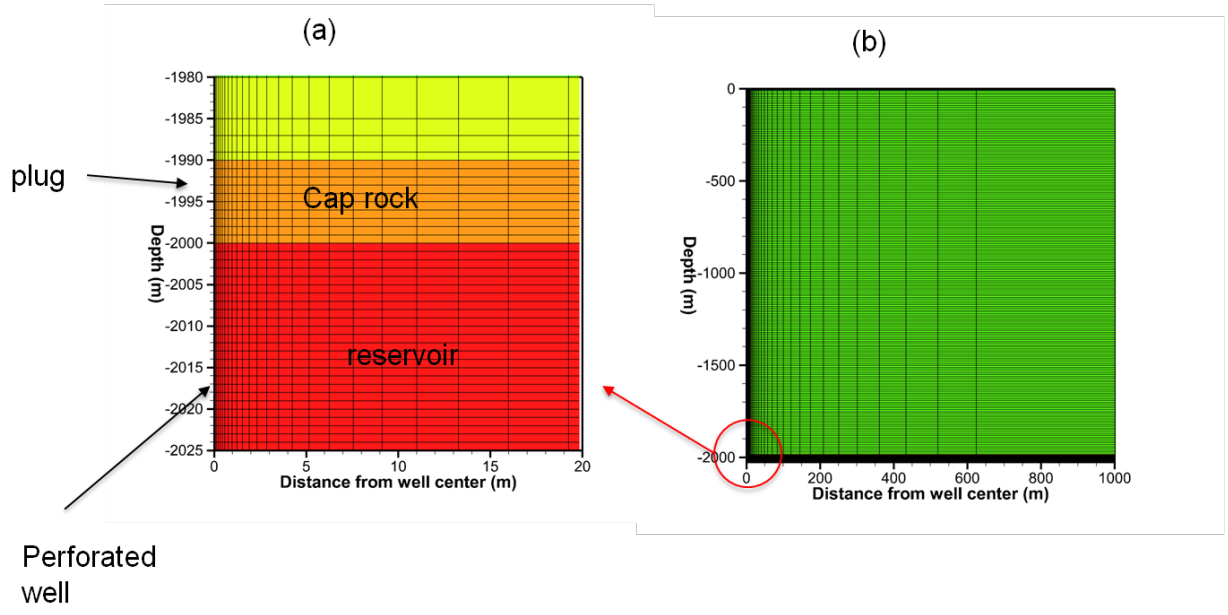

Figure 2. Radially symmetric *RZ* grid used in the simulations. Horizontal grid resolution varies from 0.1 m near well to ~200 m in the far field while the vertical resolution varies from 1 m below a depth of -1995 m (the top of the plug) to 10 m above -1985 m and 1- ~2 m near land surface. (a) locally zoomed view of the region including the well perforation zone and the plug and (b) overview of entire simulation domain.

Methods

We simulate three-phase brine-CO_2 flow in the prototypical leaking well with T2Well, a numerical simulator for solving the equations of non-isothermal, multiphase, and multi-component flows in integrated wellbore-reservoir systems (e.g., Pan et al. 2011a, b; Pan and Oldenburg, 2014). T2Well extends the numerical reservoir simulator TOUGH2 to calculate the non-Darcy flow in open (viscous) flow regions (i.e., not porous media) such as within well tubing, annuli, or cement-casing gaps and in connected porous media simultaneously and efficiently by identifying "wellbore" regions within the numerical grid in which two-phase viscous (non-Darcy) flow is simulated while generalized multiphase Darcy flow is simulated elsewhere. TOUGH2 uses a mass-conserving integral finite difference method with implicit time stepping to solve the multicomponent flow equations, and a residual-based convergence criterion with Newton-Raphson iteration to handle non-linearity (Pruess et al., 2012).

Within the wellbore sub-domains, T2Well solves a 1D momentum equation of the fluid mixture (which may be three-phase) as described by the extended drift-flux model (DFM). The velocity of the mixture is obtained by solving the momentum equation numerically while the individual phase velocities are calculated from the mixture velocity and other fluid-flow parameters as defined by the three-phase DFM. The three-phase DFM is formulated as a two-step extension of the two-phase DFM in which the two-phase DFM is first applied to get the aqueous phase velocity and the

non-aqueous (CO_2-rich) phase velocity. If the non-aqueous phase is a mixture of gas and liquid CO_2, the two-phase DFM is then applied to obtain the liquid phase velocity and gas phase velocity with proper parameters from the non-aqueous phase velocity. A mixed implicit-explicit scheme is applied to facilitate the solution of the momentum equation within the Newton-Raphson iteration framework of TOUGH2. Specifically, the pressure gradient, the gravity component, and the time-derivative of momentum are treated fully implicitly while the spatial gradient of momentum is treated explicitly. The friction term is calculated with a mixed implicit-explicit scheme (Pan et al. 2011a). Although the wellbore flow model is one-dimensional and cannot describe two- or three-dimensional flow phenomena, the drift-velocity-model implemented in T2Well does parameterize the two- or three-phase flow instabilities and turbulence and even two-phase counter-flow to model the important multiphase flow phenomena. This wellbore-domain approach is coupled seamlessly with the standard TOUGH2 porous media approach to simulate coupled wellbore-reservoir flow problems. The approach has been demonstrated over the years for problems related to wellbore leakage and injection relevant to geologic carbon sequestration (Pan et al. 2011b), oil reservoir blowout (Oldenburg et al. 2011), and gas reservoir blowout (Pan et al., 2018a). The rigor of the flow modeling in T2Well is complemented by the accuracy of the equation of state (EOS) modules used for the fluid compositions and phase relations. In this study, we make use of a research version of ECO2M (Pruess and Spycher, 2007; Pan et al., 2017) which models three fluid phases (aqueous, gaseous CO_2, and liquid CO_2), and three chemical components (H_2O, CO_2, and salt) with recent improvements and extensions (Pan et al., 2018b). ECO2M is capable of modeling three-phase aqueous systems containing gaseous, supercritical, or liquid CO_2, including two simultaneously co-existing phases of CO_2. Note that the current ECO2M has a lower limit in temperature and cannot simulate the scenarios with frozen or hydrate-forming conditions. As a result, any possible blocking of leakage due to such conditions (forming of ice or hydrate) is not considered in this study. We refer the reader to Pan and Oldenburg (2014) for a complete description of the methods used in T2Well.

Results

Introduction

Before leakage control methods can be applied, leakage must be detected and the well must be located. In order to develop and improve CO_2 and brine leakage detection and abandoned well-locating methods, it is useful to know generally what such leakage signals look like so they can be distinguished from background variations (Oldenburg et al., 2003; Cortis et al., 2008). The mechanistic simulations presented here provide information on the pressure, temperature, and fluid compositional transient signals for the case of an abandoned well leaking CO_2 and brine along a gap in a bridge plug. These results are not meant to be used for quantifying leakage rates from any particular single well nor extrapolated to estimate leakage from multiple wells because the properties of the well modeled are idealized and not site-specific. Instead, the results are meant to be used to gain insight into the signals of leakage originating by this failure mode and to explain

the mechanistic origins of the signals including their transient behaviors as a function of well system properties, with a focus on gap aperture. Insights gained from the results can be used to design monitoring and leakage quantification approaches that are especially challenging for unknown and abandoned wells.

The coupled three-phase flow system is complex resulting in the need for many figures to describe the results. We have organized the presentation into three tiers of results. The first tier summarizes the dynamic behaviors in terms of aqueous phase and CO_2-rich phase leakage rates as affected by the fracture aperture in the plug. The second tier analyzes the temporal evolution of well status in each individual well with particular aperture that causes particular characteristics in leakage behaviors. The third tier further analyzes different patterns of the friction and gravity pressure drops along the plug with different apertures which create unique characteristic leakage dynamics in the system that are very promising for leak detection.

We present in Fig. 3 the aqueous (H_2O-rich) phase and non-aqueous (CO_2-rich) phase flow rates at the top of the well for five different gap apertures. In general, the leakage starts with one or two peaks of water eruption prior to breakthrough of CO_2-rich phase. This erupted water originates as water contained in the well above the plug prior to leakage onset. As shown in Figure 3, the larger the gap aperture is, the larger the eruption strength and the earlier the eruption occurs. For example, the aqueous mass flow rate reaches 16.97 kg/s at about 130 min for the 8 mm aperture whereas the aqueous mass flow rate only reaches 1.73 kg/s at 290 min in the case of the 1 mm aperture (Figure 3a). For a 0.5 mm aperture, the aqueous phase flow starts as a strong oscillatory flow with a very small flow rate (Figure 3c). However, the magnitude of the flow rate during its single peak is larger than that in the 1 mm case although its after-peak aqueous phase flow rate is practically zero. After the short-lived transient water eruption, the aqueous phase flow rate greatly reduces to a small value associated with almost constant non-aqueous phase (CO_2-rich) flow. The non-aqueous phase (i.e., CO_2-rich phase) mass flow rate peaks immediately after breakthrough and then gradually reaches a stable value in most cases except for the cases of 1 or 2 mm gap aperture for which the early peak does not occur. The peak values of non-aqueous phase flow rate are 39.56, 13.88, 3.31 0.42, and 1.03 kg/s for gap apertures of 8, 4, 2, 1, and 0.5 mm, respectively. The corresponding stable flow rates are 32.5, 12.1, 3.3, 0.42 and 0.15 kg/s, respectively. The response in flow rate to gap-size variation is not linear.

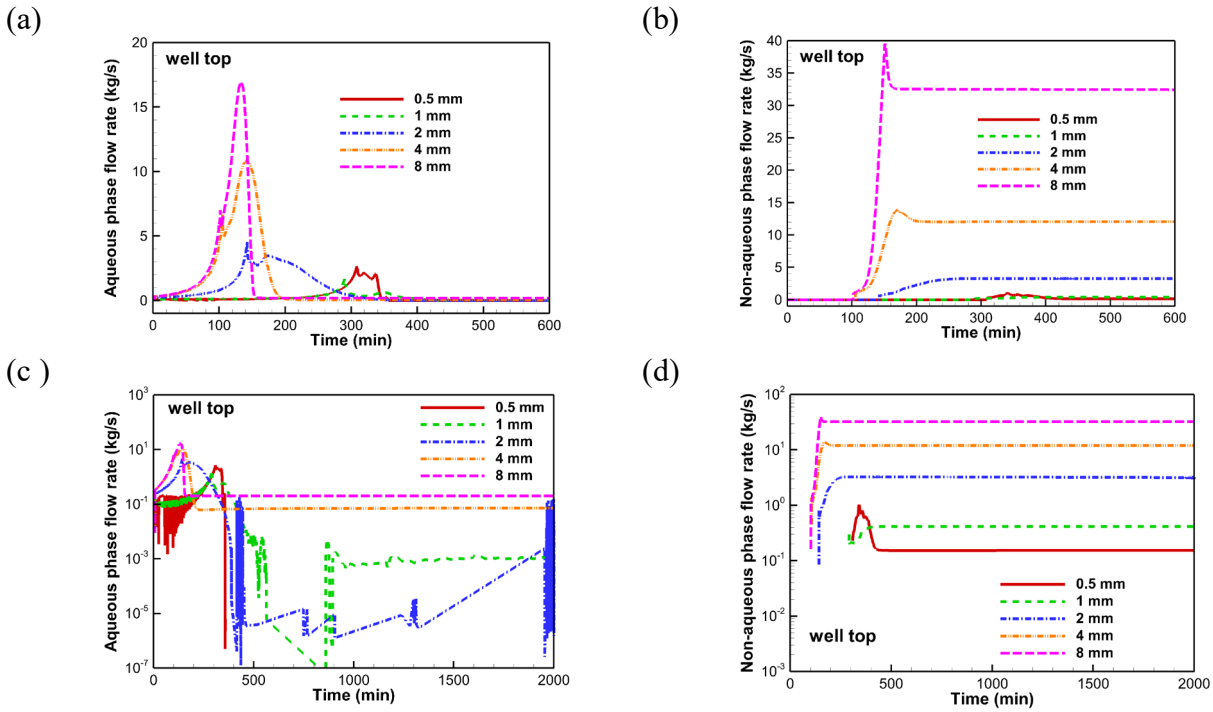

Figure 3. Simulated mass flow rates of aqueous and non-aqueous phase at the wellhead as a function of time for the five gap apertures. (a) aqueous phase flow rate, (b) non-aqueous (CO_2-rich) phase flow rate, (c) aqueous phase flow rate (log-scale) and (d) non-aqueous phase flow rate (log-scale).

The gap size does not only affect the timing and magnitude of aqueous phase eruption but it also regulates the dynamics of the aqueous phase flow rate and the final aqueous phase flow rate (Figure 3c). As shown in Figure 3c, the final aqueous phase flow rate decreases quickly with decrease of gap size for all cases in general although it does so in a manner of irregular oscillations in cases with intermediate gap size (e.g., 1 mm and 2 mm). As the aperture is reduced to 0.5 mm, the aqueous phase leakage rate is practically zero after a relatively big eruption at early time associated with the breakthrough of CO_2-rich phase.

Comparing the aqueous phase flow rate at the well top and plug top (Figure 4) reveals complicated dynamics in phase changes in the well above the plug as a function of gap aperture. For the 8 mm aperture, the aqueous phase flow rate at the wellhead (i.e., well top) is slightly higher than that at the plug top which implies that water vapor has condensed in the well above the plug (Figure 4a). This difference does not occur for the 4 mm gap in which the aqueous phase flow rates are identical at the wellhead and plug top. When the aperture is reduced to 2 mm, the aqueous phase flow rate out of the plug top is larger than that at the wellhead most of the time although the rate itself is very small. The aqueous phase leak at the wellhead for the 2 mm gap behaves more like a geyser (Figure 4a) and water may flow downward in the well during those oscillation periods. As the aperture is reduced to 1 mm, the aqueous phase flow rate at the plug top is quite stable but small after early time eruption whereas the aqueous phase flow rate at the wellhead is slightly larger with

obvious oscillations (Figure 4b). However, as the aperture is further reduced to 0.5 mm, the aqueous phase flow rate at the plug top still shows strong oscillations although they tend to decrease with time significantly (Figure 4b) while the aqueous phase flow rate at the wellhead is practically zero (Figure 3c & 4b). In smaller gap-aperture cases (1 and 0.5 mm), the aqueous phase flow rate at the plug top at early time shows strong oscillatory behavior (Figure 4b).

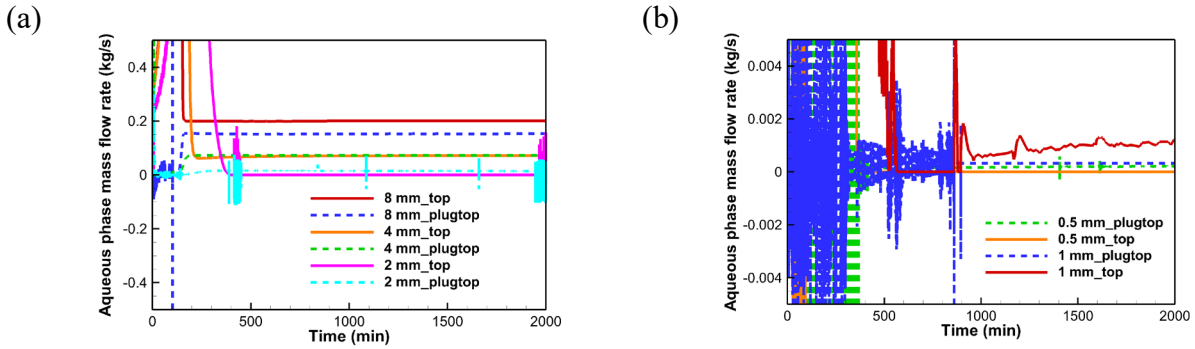

Figure 4. Simulated mass flow rates of aqueous at wellhead (top) and top of plug (plugtop) as a function of time for the four gap apertures. (a) larger aperture (8, 4, and 2 mm) and (b) smaller aperture (1 and 0,5 mm).

The complicated leakage behaviors observed to vary with gap aperture originate from variations in the non-isothermal phase change processes occurring in the well as the leakage progresses. In the following paragraphs, we will analyze the temporal evolution of aqueous phase saturation, pressure, temperature, and gaseous CO_2-ratio profiles in the well, case by case, to understand the mechanisms behind the leakage behaviors found in each case.

In the case of the 8 mm gap aperture (Figure 5a), the initially water-filled well (above 2000 m, i.e., the plug and above) becomes very dry (aqueous saturation ~0.001 or less) after 150 min because the water has been lifted out of the well by the leaking "gas" (CO_2-rich phases) in the big eruption. As a result, the pressure above the plug drops significantly after the big eruption of water (Figure 5b) although the pressure right above the plug is still around 9 MPa because of small resistance to the flow due to the large aperture (Figure 6b) and around 3.6 MPa at well top (Figure 6a). Before the water eruption, the temperature in the well increases in general as warmer fluid flows upward although the trend is complicated by the presence of CO_2-rich phase which is lighter than water (Figure 5c). The CO_2-rich phase accelerates the upward flow which brings more enthalpy from below resulting in an increase of local temperature shown as the first peak (Figure 5c) along the aqueous phase saturation line (Figure 5a or 5d). However, increases in temperature tend to be canceled or suppressed by the expansion cooling of the CO_2-rich phase as the CO_2-rich phase saturation further increases especially in shallow regions of the well until the water flow rate reaches the peak value at eruption when the CO_2-rich phase finally reaches the well top. After that the temperature above the plug drops to below 50 ºC (Figure 5c and 6d) because of expansion cooling. The temperature decreases with elevation (Figure 5c) and reaches about 3 ºC (the lower limit of the equation of state in the simulator) at the well top implying that dry ice or CO_2-hydrate

could form under this larger aperture leakage scenario. Furthermore, as shown in Figure 5d, although CO_2 transforms from supercritical to gas around the depth of 1500 m, there is a large region above the depth of 1000 m where a small amount of liquid CO_2 coexists with gaseous CO_2. This two-phase CO_2 region disappears near the top of the well (<100 m) and the continuous evaporation of liquid CO_2 at that depth is responsible for the super-cooled condition of the well above this point (the actual temperature could be lower than what is shown considering the 3 °C lower-temperature limitation of the simulator).

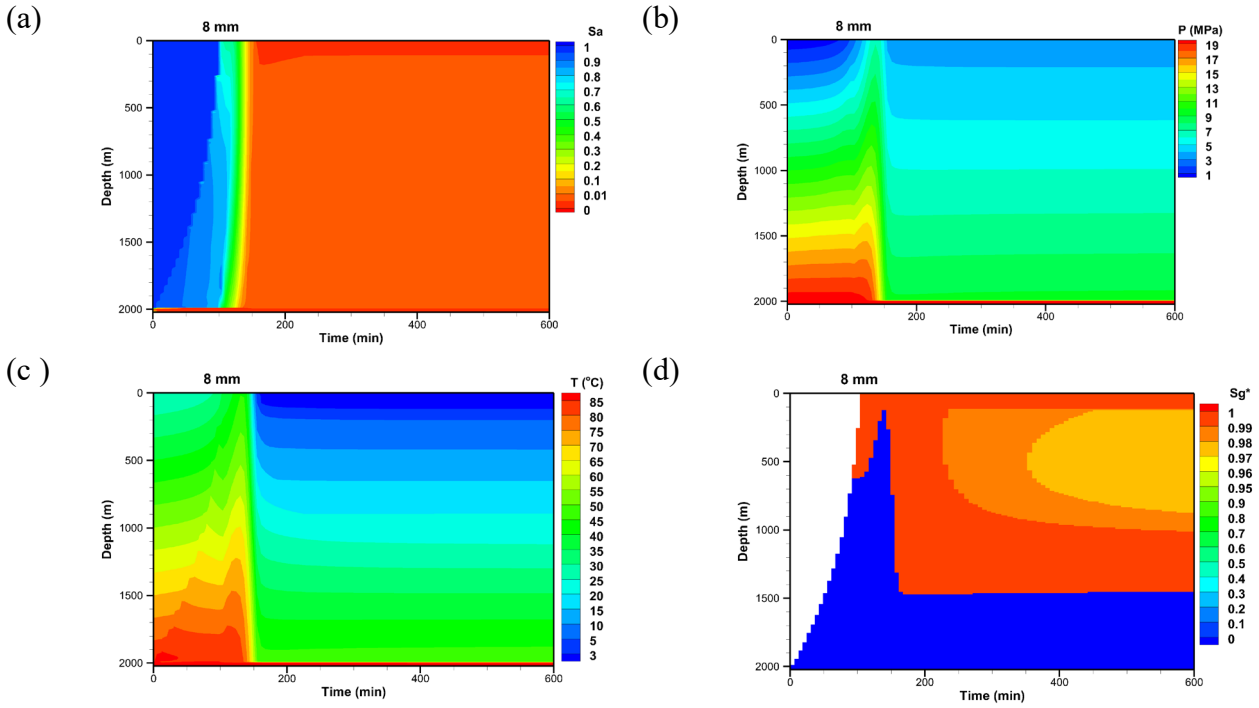

Figure 5. Evolution of profiles of (a) aqueous phase saturation, (b) pressure, (c) temperature, and (d) the ratio of gaseous CO_2 saturation within CO_2-rich phase ($Sg^* = Sg/(Sg+S_L)$, Sg is the saturation of gaseous CO_2 while S_L is the saturation of liquid or super-critical CO_2) in the well for the 8 mm gap-aperture case. The white region indicates no free CO_2 phase exists (i.e., Sa = 1).

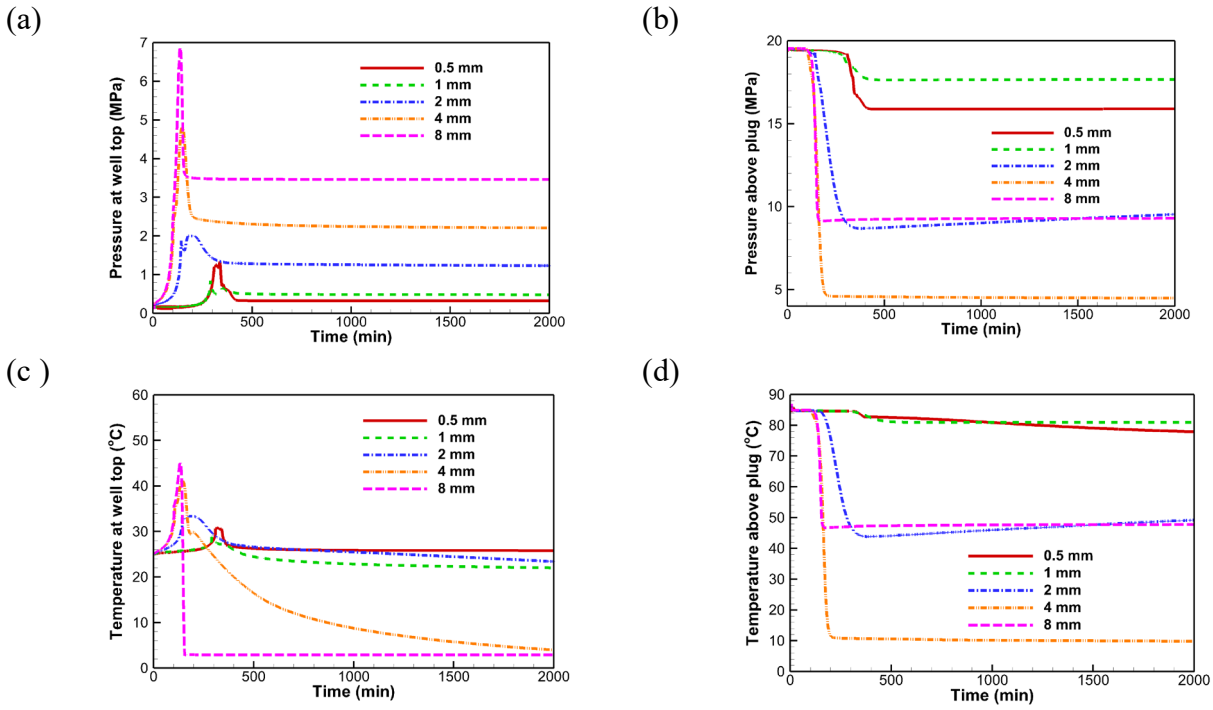

Figure 6. Simulated (a) pressure at well top, (b) pressure right above plug, (c) temperature at well top, and (d) temperature right above plug for different gap apertures.

If the 8 mm gap aperture is cut in half to 4 mm, the leaking gas is still able to flush the water out of the well to make a very dry well although it takes about 30 min longer time to do so (Figure 7a). The pressure drop after the water eruption is more severe for the 4 mm gap than for the 8 mm gap (Figure 7b) because of the larger resistance to leakage flow through the smaller (4 mm) aperture. The pressure right above the plug is reduced to 4.5 MPa while the well top pressure drops to 2.2 MPa (Figure 6b, 6a), and pressures at both of these locations are significantly lower than those in the 8 mm case. Although the evolution of the temperature profile before the water eruption for the 4 mm gap has a similar pattern to that for the 8 mm gap, differences are quite large overall between the two cases (Figure 6c and 7c). Whereas the coldest point in the 8 mm case is located at the well top, the coldest point in the 4 mm case is located at about a depth of 1500 m at 600 min, near the upper margin of the two-phase CO_2 region (Figure 7d). By close inspection of the Sg* (Sg* = Sg/(Sg+Sl) plot (not shown here), we observed that CO_2 evolves from supercritical conditions to enter a two-phase region before reaching the top of the plug in the 4 mm gap-aperture case. The CO_2 temperature continues to decrease as it flows upward because of the drop in pressure (along the phase line). After CO_2 passes the upper margin of the two-phase region, expansion cooling causes further drop in gas temperature. As gaseous CO_2 migrates farther upward, the heat from the surrounding formations is able to overcome the expansion cooling resulting in a gradual increase in temperature as CO_2 flows up to the well top. However, this formation-to-well heating effect is weakening with time so that the cold region shown in Figure 7c gradually expands upward and reaches the well top at about 2400 min (not shown here) and the well top temperature is eventually

1 approaching 3ºC (Figure 6c) although the temperature right above the plug is stabilized at 10 ºC
2 after 200 min (Figure 6d).

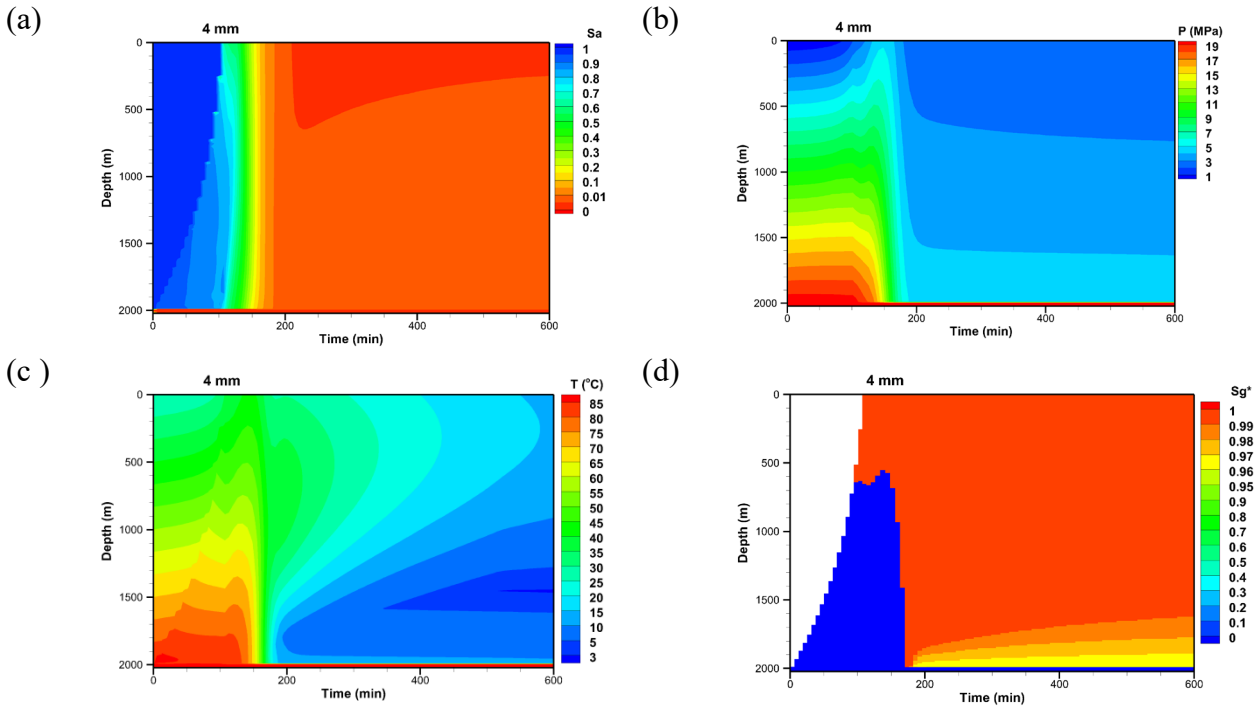

Figure 7. Evolution of profiles of (a) aqueous phase saturation, (b) pressure, (c) temperature, and (d) the ratio of gaseous CO_2 saturation within CO_2-rich phase ($Sg^* = Sg/(Sg+S_L)$, Sg is the saturation of gaseous CO_2 while S_L is the saturation of liquid or super-critical CO_2) in the well for the 4 mm case. The white region indicates no free CO_2 phase exists (i.e., Sa = 1).

For the 2 mm gap aperture, the leaking gas is not able to lift all of the water above the plug out of well, unlike in the cases with larger aperture (e.g., 4 and 8 mm). As shown in Figure 8a, significant aqueous phase still exists in the well after the water eruption around 200 min. Such phase conditions are reflected in the pressure profiles as shown in Figure 8b. The aqueous phase (denser than CO_2) increases the gravitational pressure gradient along the well. As a result, although the well top pressure is about 1.3 MPa in the 2 mm case, much smaller than 2.2 MPa in 4 mm case or 3.6 MPa in 8 mm case (Figure 6a), the pressure right above the plug for the 2 mm gap-aperture case is around 9 MPa (Figure 6b), a level similar to that in 8 mm case, and is much higher than that in 4 mm case (~4.5 MPa). While the well-top pressure is mainly controlled by the final leakage rate, the pressure right above the plug is a result of two interacting factors, the pressure drop through the plug corresponding to the given flow rate from below and the gravity force asserted by the water column in the well above the plug. The significant aqueous phase in the well also alters the temperature profile in the 2 mm case (Figure 8c). Although the temperature right above the plug drops to below 50 ºC due to expansion cooling (Figure 6d), similar to the 8 mm case, the smaller CO_2-rich aqueous phase saturation (which is under expansion cooling) and smaller leakage rate in the 2 mm case make it possible for the upward flowing fluid to be heated up by the surrounding formations especially in the region below 1000 m (Figure 8c). As a result, the well top temperature in the 2 mm case is close to the ambient temperature although it is slowly decreasing with time (Figure 6c) as the surrounding formations gradually cool. Different from the 4 mm case, no two-phase CO_2 regions occur in the 2 mm case (Figure 8d). Instead, the CO_2 transitions from supercritical into gaseous phase at 1800 m depth.

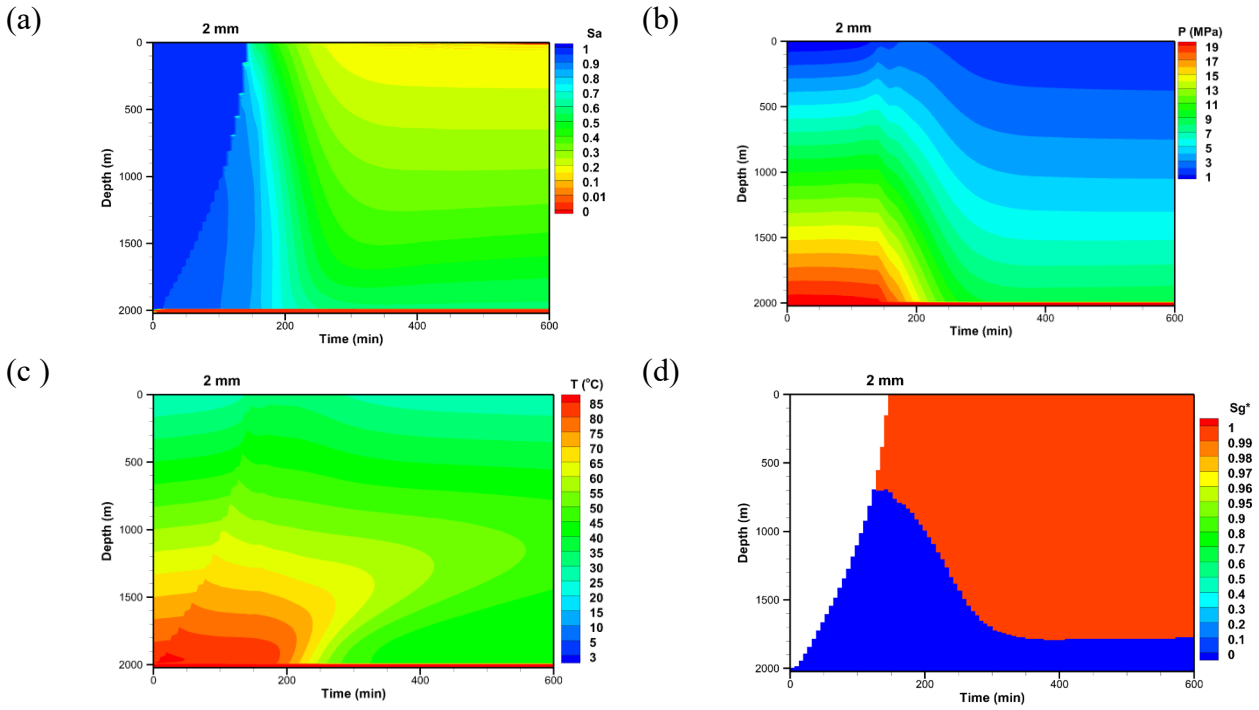

Figure 8. Evolution of profiles of (a) aqueous phase saturation, (b) pressure, (c) temperature, and (d) the ratio of gaseous CO_2 saturation within CO_2-rich phase ($Sg^* = Sg/(Sg+S_L)$, Sg is the saturation of gaseous CO_2 while S_L is the saturation of liquid or super-critical CO_2) in the well for the 2 mm case. The white region indicates no free CO_2 phase exists (i.e., Sa = 1).

As the fracture aperture reduces to 1 mm, the resistance to leakage through the gap increases. As a result, the leakage rate of CO_2-rich phase only reaches about 0.42 kg/s (Figure 3b and 3d). Although there are two small peaks of aqueous phase flow at the well top associated with the breakthrough of CO_2-rich phase (Figure 3a and 3c), the leaking CO_2 is just not able to lift much water out of the well resulting in a very wet well (high aqueous phase saturation) in the 1 mm case (Figure 9a). Consequently, the pressure gradient in the well (the section above the plug) is only slightly increased from the ambient hydrostatic pressure gradient due to leaking CO_2 (Figure 9b). The pressure right above the plug only drops by 1.8 MPa to 17.6 MPa (Figure 6b) while the well-top pressure is slightly below 0.5 MPa (Figure 6a). The temperature profile changes little except for the small peak that occurs associated with the initial rise of CO_2-rich phase (Figure 9c). The CO_2 converts from supercritical into gaseous at a depth of 850 m (Figure 9d) which is about 950 m shallower than that in the 2 mm case.

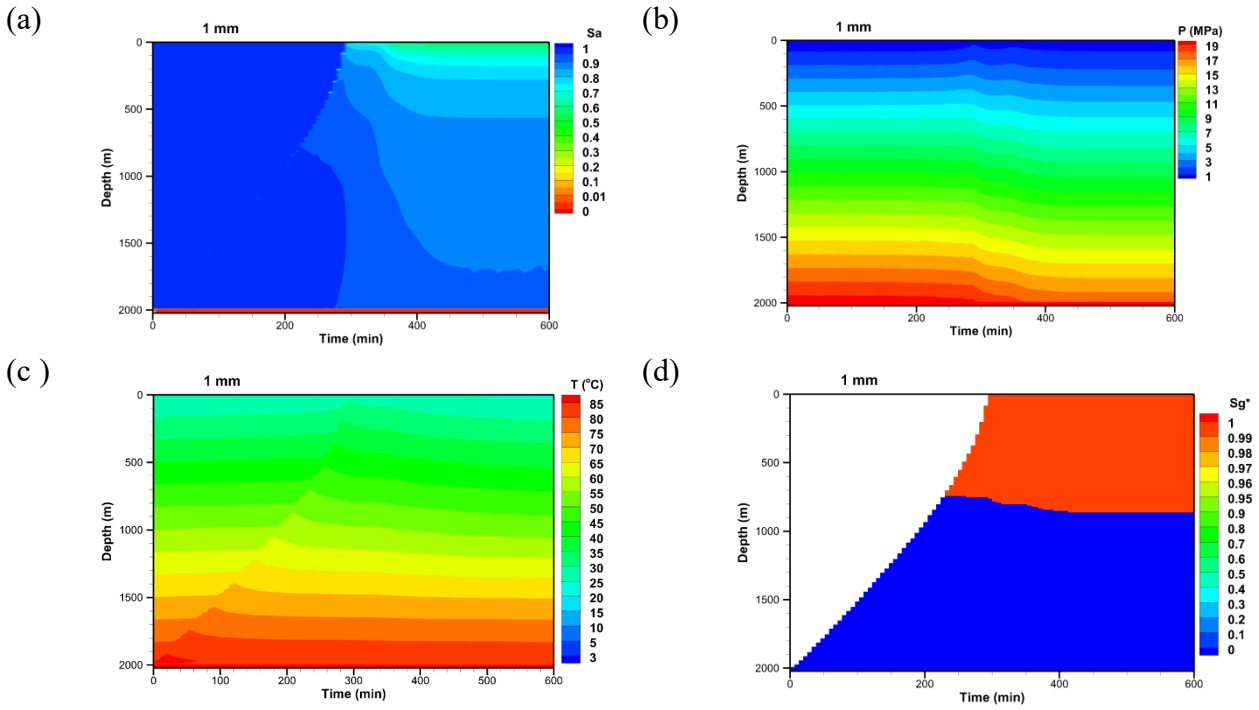

Figure 9. Evolution of profiles of (a) aqueous phase saturation, (b) pressure, (c) temperature, and (d) the ratio of gaseous CO_2 saturation within CO_2-rich phase ($Sg^* = Sg/(Sg+S_L)$, Sg is the saturation of gaseous CO_2 while S_L is the saturation of liquid or super-critical CO_2) in the well of 1 mm case. The white region indicates no free CO_2 phase exists (i.e., Sa = 1).

As gap aperture further reduces to 0.5 mm (five times the 100 micron roughness of the gap walls), the steady-state leakage rate of the CO_2-rich phase is only 0.15 kg/s (Figure 3b and 3d), which can barely lift any water out of the well top after the early oscillatory period ends as shown in Figure 3c or 4b. However, the CO_2 bubbles seem to accumulate to a significant level (Figure 10a) to cause an eruption of aqueous phase larger than that in the 1 mm case (Figure 3a). After that, a stable water table at a depth of 260 m forms implying that the flow becomes a scenario of rising CO_2 bubbles through an almost static water column. This can be seen in Figure 4b where the aqueous phase flow rate at the well top is zero and at the top of the plug is very small with occasional downward flow peaks in the 0.5 mm case, which is different from the 1 mm case where a continue upward aqueous flow exists although at very small magnitude or in a somewhat oscillatory way. The pressure after early eruption is lower in the 0.5 mm case than that in the 1 mm case (Figure 10b and 9b) although the temperature profiles are very similar (Figure 10c and 9c). The turning point between gaseous and supercritical CO_2 is located at a depth of 1100 m which is deeper than that in the 1 mm case but shallower than that in the 2 mm case (Figure 10d, 9d, and 8d).

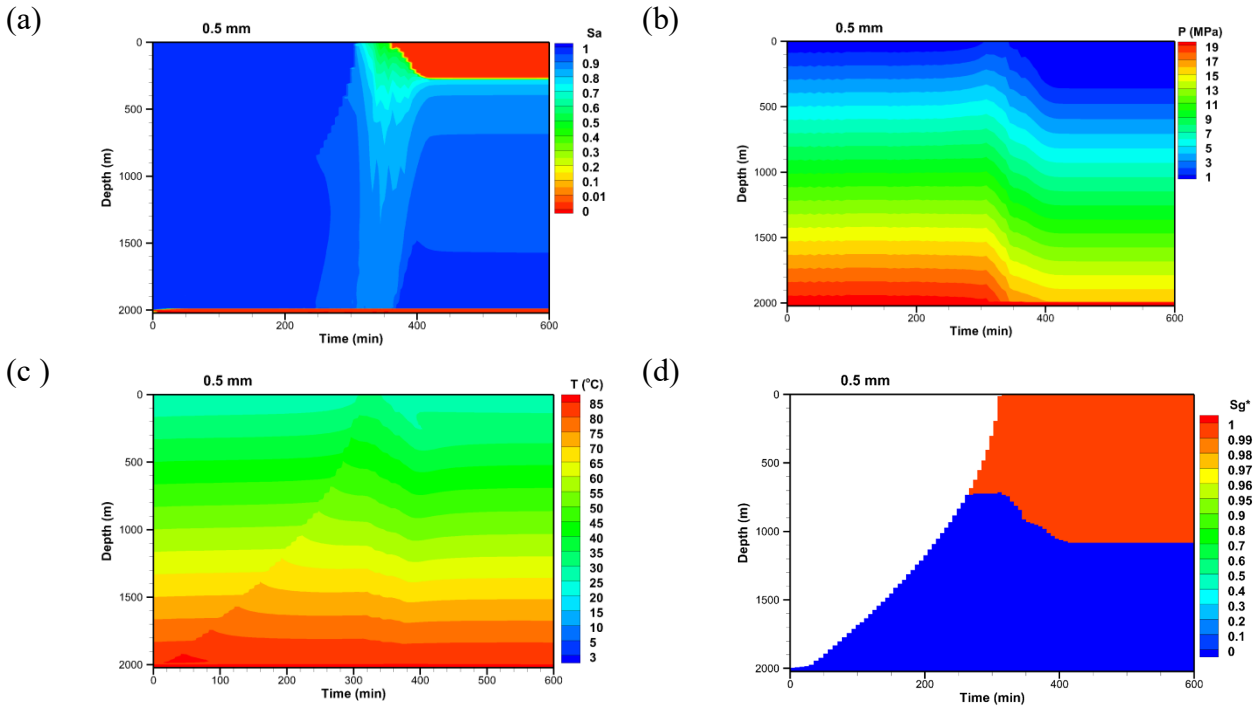

Figure 10. Evolution of profiles of (a) aqueous phase saturation, (b) pressure, (c) temperature, and (d) the ratio of gaseous CO_2 saturation within CO_2-rich phase ($Sg^* = Sg/(Sg+S_L)$, Sg is the saturation of gaseous CO_2 while S_L is the saturation of liquid or super-critical CO_2) in the well of 0.5 mm case. The white region indicates no free CO_2 phase exists (i.e., Sa = 1).

The gap in the plug is a narrow flow path which is quite different from the open well above and below the plug from the perspective of flow resistance. We will now inspect the various components of the pressure loss in the plug gap as compared to those in the open well to capture the insights of flow dynamics within the plug. As shown in Figure 11, the friction loss is orders of magnitude higher than the gravity pressure loss through the plug gap whereas the former is often a fraction of the latter in the well above or below the plug (Figure 11 a and b). In the open-well section (above or below the plug), the friction loss (Figure 11a) is directly proportional to the mixture velocity squared (Figure 11e) because the wall roughness is so small (45 microns) compared to the well diameter (16 cm). However, in the plug gap, because the flow path is very narrow (0.5-8 mm) compared to the wall roughness (0.1 mm), the larger relative roughness (the ratio of wall roughness to the size of the flow path) starts to alter the relationship between the friction loss and the mixture velocity. For example, although the mixture velocity for the 4 mm gap aperture is smaller than that in the 8 mm case in most of the plug gap (Figure 11e), the friction loss within the plug in the 4 mm case is significantly larger than that in 8 mm case (Figure 11a, notice the log scale). Furthermore, even though the mixture velocity within the plug for the 2 mm gap aperture is about a quarter of that in the 8 mm case, the friction loss within the plug is about the same in these two cases. As the aperture is reduced more toward the value of the roughness, although the mixture velocity within the plug in the 1 mm case is slightly larger than that in the 0.5 mm case, the friction loss in the 0.5 mm case is significantly larger than that in the 1 mm case. In reality, the wall roughness, not to mention the aperture, of a gap between cement and casing or

of a fracture in the cement plug may be spatially variable resulting in leakage flow behaviors more complicated than those revealed in these idealized simulations.

The gravity pressure loss (Figure 11b) reflects the fluid density changing with depth. Except for the 4 mm case, the CO_2 within the plug remains in supercritical state as it was in the reservoir (Figure 11d). As a result, the gravity pressure loss within the plug increases with the gap aperture in these cases because the total pressure loss is proportional to the fracture aperture in the plug in general. The existence of significant aqueous phase in the upper portion of the plug in the smaller aperture cases (2, 1, and 0.5 mm) greatly increases the density of fluid (water-CO_2 mixture) thereby increasing the gravity pressure loss there. In the 4 mm case, larger friction loss causes the pressure in the upper portion of the plug to drop to subcritical levels so that CO_2 there becomes two-phase (Figure 11d). The transition to gaseous CO_2 greatly reduces the density of the fluid mixture which leads to the smallest gravity pressure loss (Figure 11b) and the largest mixture velocity (Figure 11e) in the upper region of the plug gap. The occurrence of two-phase CO_2 also greatly decreases the temperature there in the 4 mm case (Figure 11f). As a result, the temperature at the top of the plug in the 4 mm case decreases to below 10 ºC which is about 40 ºC below the cases of the 2 mm and 8 mm gap apertures and 70 ºC below the 1 mm and 0.5 mm cases.

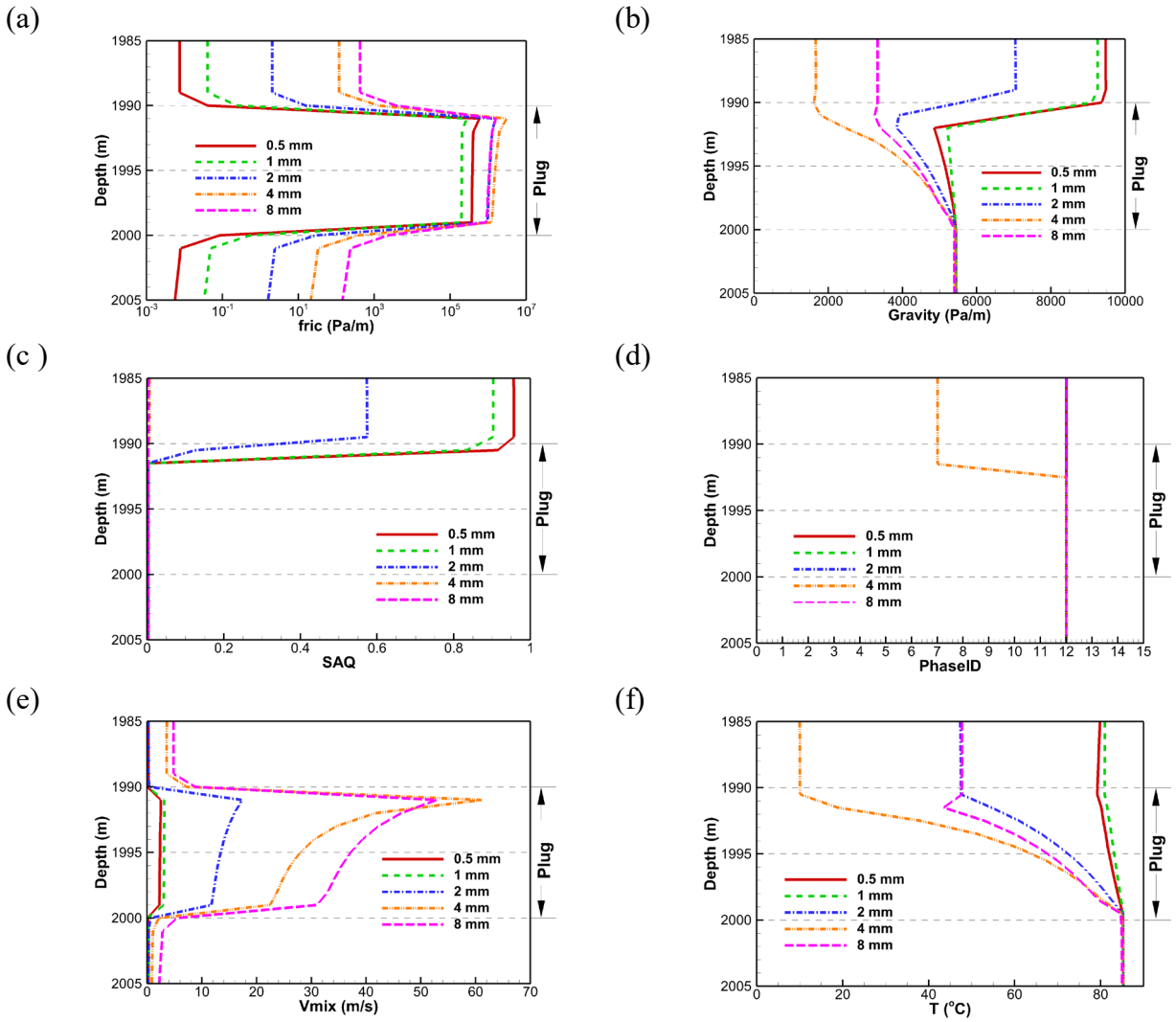

Figure 11. Profiles of (a) friction pressure gradient, (b) gravity pressure gradient, (c) aqueous phase saturation, (d) Phase ID (12—supercritical CO_2-Aqueous, 7—three phases), (e) mixture velocity, and (f) temperature along the plug (1990-2000 m) at 1440 min (1 day).

Discussion

Discussion of results relative to detection of well leakage

The gap between the cement plug and casing, or an equivalent fracture in the plug, is the limiting feature (bottleneck) for flow of CO_2 leaking up within casing of an abandoned well. In the case of a relatively large aperture (e.g., 4 or 8 mm), the plug offers little resistance to the leaking CO_2. In these cases of minimal flow resistance for sudden opening of the gap, the leaking CO_2 is able to lift the water originally residing in the well above the plug out of the well in a manner of an eruption (Figure 5a and 7a). After this initial phase of leakage, water plays little role in regulating the leakage of CO_2 and expansion cooling of CO_2 along the well makes the temperature near the land

surface very low, possibly below 3 ºC (As shown in Figure 6c, temperature at the top reached the lower limit of the equation of state in our simulator). Such abnormally low temperatures could be a convenient signal of leakage because of the relative ease of measuring temperature over areas of the ground surface. For example, Figure 12 shows the temperature deviation from the ambient temperature in the top (1 m) portion of the soil as a function of horizontal distance from the well at the end of 1 day. As shown in Figure 12, the larger aperture cases (4 and 8 mm) not only have larger temperature drop (> 20 ºC) but also a larger anomalously cold region (3-4 m in radius) which provides a promising basis for detecting leaking abandoned wells with soil cover by thermal mapping tools. However, as the aperture decreases, both the cold area and the magnitude of the temperature drop decrease. Especially in the case of 0.5 mm, the maximum temperature drop is about 2 ºC and the radius of the cold area is only a fraction of a meter. This is because the CO_2 leakage rate is so low in the 0.5 mm case (Figure 3b) that the flow is unable to lift significant water out of the well (Figure 10a). Although the CO_2 bubbles are still undergoing expansion cooling as they slowly migrate upward through the water column, the cooling effects of the limited quantity of CO_2 are not enough to cause a large temperature drop in the soil above the well (Figure 12). The water in the well above the plug becomes an effective barrier for the CO_2 leakage in these small-aperture cases (e.g., 1 and 0.5 mm) by exerting a large pressure on the top side of the plug which greatly reduces the pressure gradient through the plug that drives the upward CO_2 flow.

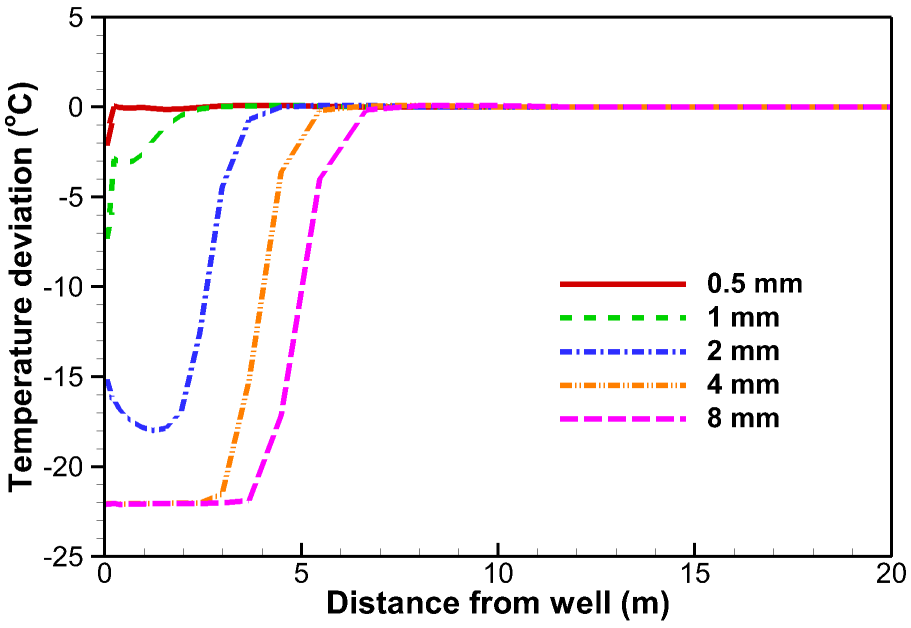

Figure 12. Temperature deviations from the ambient temperature in top soil above the well as a function of horizontal distance from the well center at 1440 min (1 day).

The effects of water on the CO_2 leakage become more complicated in the case of the medium-aperture gap (2 mm) because the CO_2 leakage rate is large enough to lift some water out of the well resulting in lower water saturation in the well than the smaller-aperture cases but not a dry

well as in larger-aperture cases (Figure 8). As a result, the two-phase interactions between the aqueous phase and the CO_2-rich phase create complicated oscillations in the flow of both the aqueous phase and CO_2-rich phase (Figure 13). These oscillations in flow and temperature at the top of the well may be a useful target for monitoring for well leakage because they may stand out from natural cycles driven by atmospheric pressure, diurnal effects, or precipitation and runoff. As shown in Figure 13, for most of the time the oscillations at the plug top are stronger than those at the well top, except for occasional eruption events (e.g., at around 400 min and 2000 min), implying that the well section above the plug acts as a buffer capable of smoothing out the oscillations. During that period, the water flows upward and downward alternately (Figure 13c) within the well, indicating alternately dominant gas lift (causing upward water flow) and gravity (causing downward water flow) effects. Such alternate upward-downward water flow in the 2 mm case shown in Figure 13c does not occur or becomes less significant after a certain time as we observed in other cases (not shown here). In larger-aperture cases (4 or 8 mm), almost all of the water is lifted out of the well by the leaking gas within a few hundred minutes resulting in a gas-phase dominant flowing well in which the two-phase interaction is minimum (i.e., small amount of condensed water becomes mist dispersed in gas stream). On the other hand, in smaller aperture cases (1 or 0.5 mm), the gas flow becomes bubble flow through an almost static water column after early time in which the magnitude of water flow caused by the bubble flow is very small. In the 1 mm gap-aperture case, there are some oscillations in magnitude of the upward water flow rate at the well top as shown in Figure 4b.

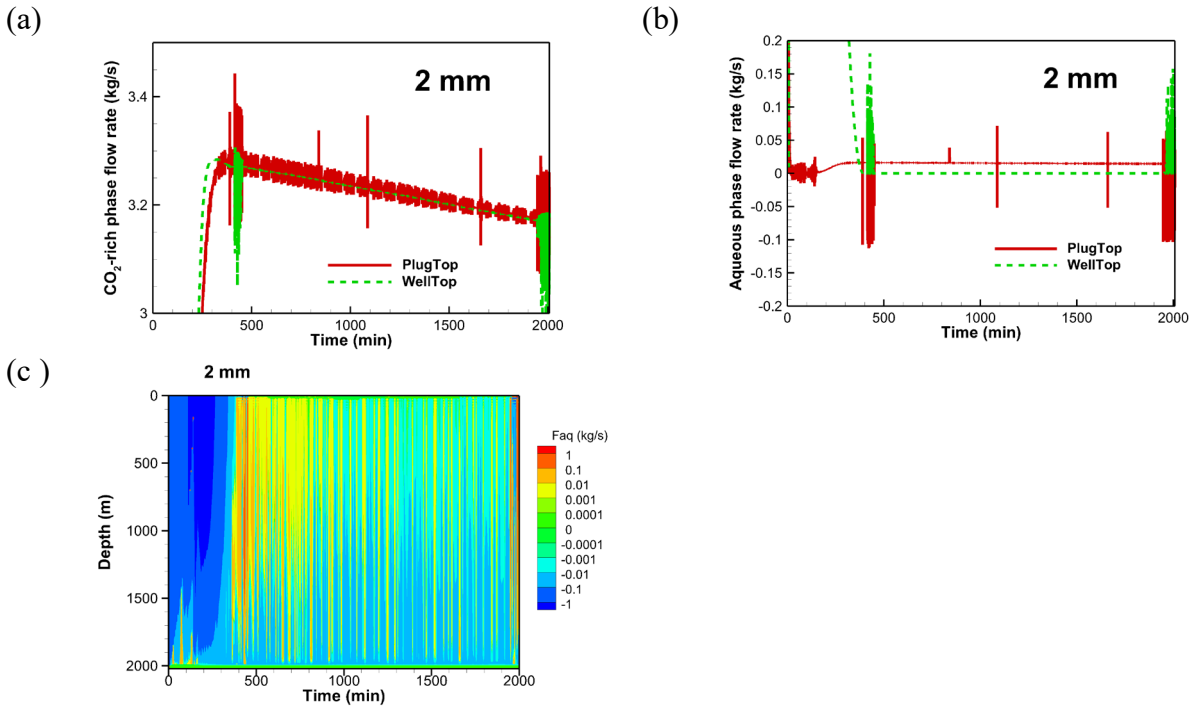

Figure 13. Evolution of flow rate in 2 mm case: (a) CO_2-rich phase flow rates through well top and plug top, (b) aqueous phase flow rates through well top and plug top, (3) contours of aqueous phase flow rate over depth-time space (positive indicating upward flow and negative indicating downward flow).

Assuming an abandoned well can be located, monitoring the pressures in the well may be an effective way to detect leakage. As shown in Figure 6a and 6b, the well top pressure will increase and the plug top pressure will decreases significantly in response to leakage past a bridge plug. The pressure monitoring can detect plug failure even if no CO_2 is released to the atmosphere in the case that the cap of the abandoned well is an effective seal. Of course, the cost to install such monitoring system may be high if large number abandoned wells are involved.

Discussion of results relative to effects of plug length on leakage

In this study, we conceptualize a prototypical abandoned well system with a 10 m-long plug, which is only about 1/3 of the length required by current U.S. regulation. To understand the effects of the plug length on the leakage dynamics in a failed abandoned well, we performed another set of simulations in which the plug length is changed to 30 m but everything else stays the same. As shown in Figure 14, a longer plug results in smaller leakage rates in both the 8 mm and 4 mm cases relative to the 10 m-long plug. However, the patterns are similar regardless of plug length. Similar trends can be seen in smaller aperture cases (not shown here). Furthermore, the leakage rate is more sensitive to the aperture than to plug length (Figure 15). For example, the final (stable) CO_2 leakage rate in the 8 mm case with 10 m-long plug is about 32.3 kg/s. If the plug length increases to 30 m (3 times), the CO_2 leakage rate reduces to about 23.3 kg/s, about 72% of the original value. However, if the aperture reduces to 4 mm (a half) with the same plug length, the CO_2 leakage rate would reduce to 12.1 kg/s, about 37%. This is because increase of plug length only increases the

resistance to the flow linearly whereas decrease of aperture not only increases the friction through the friction coefficient but also through increase in velocity for the same mass flow rate which would increase the friction proportional to velocity squared.

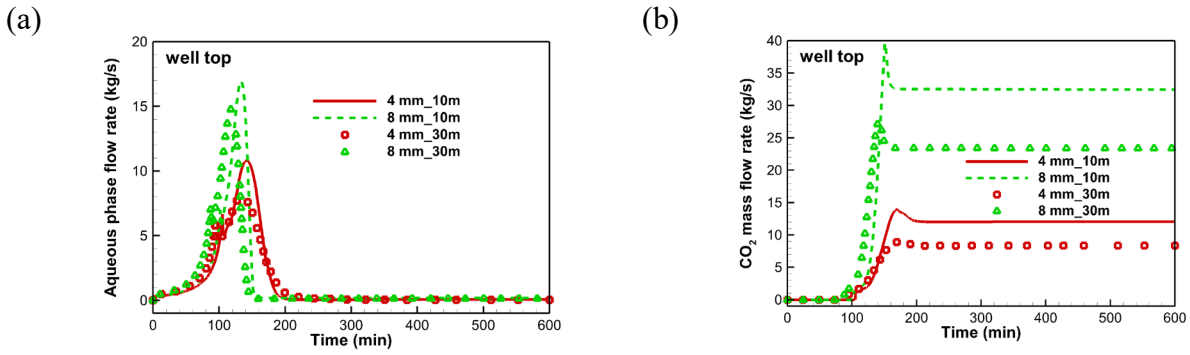

Figure 14. Comparison of the simulated mass flow rates of aqueous (a) and non-aqueous phase (b) at the wellhead as a function of time for two big gap apertures with different plug length.

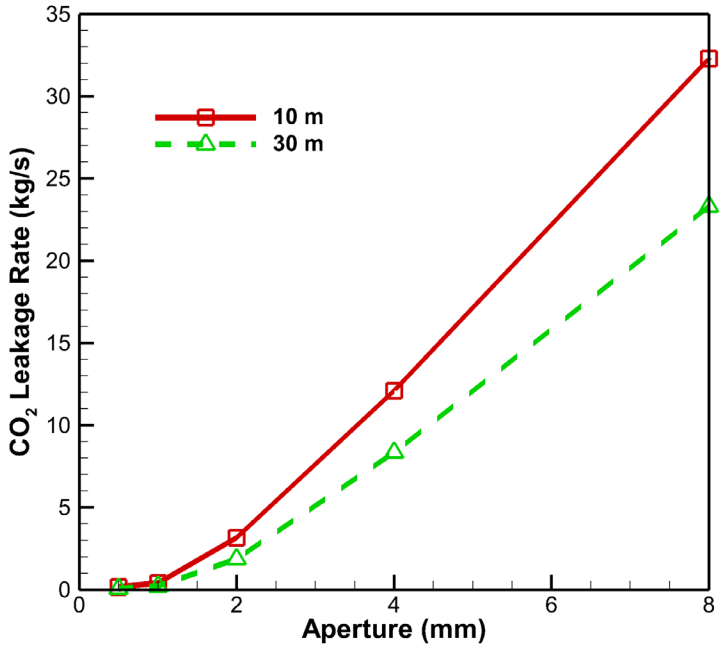

Figure 15. Comparison of the final CO_2 leakage rates as a function of aperture for two plug lengthes.

Conclusions

We have used T2Well to simulate the non-Darcy non-isothermal three-phase (aqueous, liquid-CO_2, and gas-CO_2) flow of CO_2 and brine in a prototypical abandoned well suffering a sudden failure of a cement plug during the post-injection period at a GCS site. Results show transient

leakage rate and signals of pressure, temperature, and saturation at the top of the well as a result of complicated CO_2-water interactions in the open well sections and in the gap or fracture of a bridge plug. The leakage signals and flow rate show strong dependence on gap aperture. The leakage rate increases with the aperture of the fracture in the plug greatly. In larger aperture cases, the water in the well above the plug will be lifted out of the well by the leaking CO_2, resulting in a dry well in which CO_2 flows freely without interference of the aqueous phase. In these cases the CO_2 expansion cooling effect is extremely strong resulting in a significant cold area around the well forms at land surface which implies that thermal mapping could be an effective monitoring technique to detect possible leakage from abandoned wells. While short-lived two-phase CO_2 regions occur in the 8 mm gap-aperture case, the two-phase CO_2 region exists consistently at the top of the plug (as well as the nearby section above the plug) in the 4 mm case. The strong cooling due to evaporation of the liquid CO_2 in addition to expansion cooling of gaseous CO_2 in the 4 mm case makes the cold region start at the plug and gradually expand to the land surface. For smaller apertures, both the magnitude of the temperature drop and the size of the cold area at the land surface decrease with aperture because the amount of the leaking CO_2 decreases and water saturation increases. As in the 0.5 mm case, such cooling signals become very weak.

During the period with strong interaction between aqueous phase and CO_2-rich phase (usually at early time), the water flow direction can be oscillatory (up and down) at different depths within the well section above the plug, especially in the case of intermediate aperture (e.g., 2 mm) in which case the oscillations never end. In this case, the transient pressure, temperature, and flow rate signals from such a system may stand out from variations arising from natural forcings (barometric pressure, day-night, weather) at the ground surface and provide target strategies for leakage detection monitoring. Furthermore, analysis of the leakage signals may allow diagnosis of the cause and/or source of leakage, characteristics of the flow channel (e.g., its aperture, etc.) that can potentially inform remediation efforts.

The results also show that the well top pressure will increase and the plug top pressure will decrease significantly in response to the leakage. Therefore, pressure monitoring in abandoned wells is an effective way to detect potential leakage although deployment of such monitoring system may be costly if large number of wells are involved.

ECO2M has a lower limit on temperature and cannot simulate scenarios of water ice conditions or hydrate-forming conditions which may interfere or even block further CO_2 leakage in some cases. Therefore, the leakage behaviors may be very different from those reported here if such conditions occur.

Acknowledgment

This work was completed as part of the National Risk Assessment Partnership (NRAP) project. Support for this work was provided by the Office of Fossil Energy (DOE), under its Office of Coal CO_2 Sequestration R&D Program, through the National Energy Technology Laboratory (NETL),

and by Lawrence Berkeley National Laboratory under Department of Energy Contract No. DE-AC02-05CH11231.

References

Bachu, S. and Bennion, D.B., 2009. Experimental assessment of brine and/or CO_2 leakage through well cements at reservoir conditions. International Journal of Greenhouse Gas Control, 3(4), pp.494-501.

Brunet, J.P.L., Li, L., Karpyn, Z.T. and Huerta, N.J., 2016. Fracture opening or self-sealing: Critical residence time as a unifying parameter for cement–CO 2–brine interactions. International Journal of Greenhouse Gas Control, 47, pp.25-37.

Bourgoyne, A.T., Scott, S.L. and Regg, J.B., 1999, January. Sustained casing pressure in offshore producing wells. In *Offshore Technology Conference*. Offshore Technology Conference.

Carey, J.W., Svec, R., Grigg, R., Zhang, J. and Crow, W., 2010. Experimental investigation of wellbore integrity and CO_2–brine flow along the casing–cement microannulus. International Journal of Greenhouse Gas Control, 4(2), pp.272-282.

Celia, M.A., Bachu, S., Nordbotten, J.M., Gasda, S.E. and Dahle, H.K., 2005. -Quantitative estimation of CO 2 leakage from geological storage: Analytical models, numerical models, and data needs. In Greenhouse Gas Control Technologies 7 (pp. 663-671).

Choi, Y.S., Young, D., Nešić, S. and Gray, L.G., 2013. Wellbore integrity and corrosion of carbon steel in CO_2 geologic storage environments: A literature review. International Journal of Greenhouse Gas Control, 16, pp.S70-S77.

Cortis, A., Oldenburg, C.M. and Benson, S.M., 2008. The role of optimality in characterizing CO_2 seepage from geologic carbon sequestration sites. International Journal of Greenhouse Gas Control, 2(4), pp.640-652.

Crow, W., Carey, J.W., Gasda, S., Williams, D.B. and Celia, M., 2010. Wellbore integrity analysis of a natural CO_2 producer. International Journal of Greenhouse Gas Control, 4(2), pp.186-197.

Ebigbo, A., Class, H. and Helmig, R., 2007. CO 2 leakage through an abandoned well: problem-oriented benchmarks. Computational Geosciences, 11(2), pp.103-115.

Gasda, S.E., Bachu, S. and Celia, M.A., 2004. Spatial characterization of the location of potentially leaky wells penetrating a deep saline aquifer in a mature sedimentary basin. *Environmental geology*, *46*(6-7), pp.707-720.

Grace, R.D., 2017. Blowout and well control handbook. Gulf Professional Publishing.

Huerta, N.J., Hesse, M.A., Bryant, S.L., Strazisar, B.R. and Lopano, C.L., 2012. Experimental evidence for self-limiting reactive flow through a fractured cement core: implications for time-dependent wellbore leakage. Environmental science & technology, 47(1), pp.269-275.

Kutchko, B.G., Strazisar, B.R., Dzombak, D.A., Lowry, G.V. and Thaulow, N., 2007. Degradation of well cement by CO2 under geologic sequestration conditions. *Environmental science & technology*, *41*(13), pp.4787-4792.

Lackey, G., Rajaram, H., Sherwood, O.A., Burke, T.L. and Ryan, J.N., 2017. Surface casing pressure as an indicator of well integrity loss and stray gas migration in the Wattenberg Field, Colorado. *Environmental science & technology*, *51*(6), pp.3567-3574.

Lynch RD, McBride EJ, Perkins TK, Wiley ME. Dynamic kill of an uncontrolled CO_2 well. journal of Petroleum Technology. 1985 Jul 1;37(07):1-267.

NPC (National Petroleum Council), Technology Subgroup of the Operations & Environment Task Group), PLUGGING AND ABANDONMENT OF OIL AND GAS WELLS, White paper #2-25, 2011.

Nordbotten, J.M., Celia, M.A. and Bachu, S., 2004. Analytical solutions for leakage rates through abandoned wells. Water Resources Research, 40(4).

Nordbotten, J.M., Celia, M.A., Bachu, S. and Dahle, H.K., 2005. Semianalytical solution for CO_2 leakage through an abandoned well. Environmental science & technology, 39(2), pp.602-611.

Nordbotten, J.M., Kavetski, D., Celia, M.A. and Bachu, S., 2008. Model for CO_2 leakage including multiple geological layers and multiple leaky wells. Environmental science & technology, 43(3), pp.743-749.

Oldenburg, C.M., Jordan, P.D., Nicot, J.P., Mazzoldi, A., Gupta, A.K. and Bryant, S.L., 2011. Leakage risk assessment of the In Salah CO_2 storage project: Applying the certification framework in a dynamic context. Energy Procedia, 4, pp.4154-4161.

Oldenburg, C.M., Lewicki, J.L. and Hepple, R.P., 2003. Near-surface monitoring strategies for geologic carbon dioxide storage verification, Lawrence Berkeley National Laboratory Report LBNL-54089. https://escholarship.org/uc/item/1cg241jb

Pan L, Lewicki JL, Oldenburg CM, Fischer ML. Time-window-based filtering method for near-surface detection of leakage from geologic carbon sequestration sites. Environmental Earth Sciences. 2010 Mar 1;60(2):359-69.

Pan, L., C.M. Oldenburg, Y.-S. Wu, and K. Pruess, Transient CO_2 leakage and injection in wellbore-reservoir systems for geologic carbon sequestration, Greenhouse Gases: Sci. and Tech., 1(4), 335-350, 2011. LBNL-5248E.

Pan, L., and C.M. Oldenburg. "T2Well—An integrated wellbore–reservoir simulator." Computers & Geosciences 65 (2014), 46-55.

Pan, L. and Oldenburg, C.M., 2016. Reduced-Order Model for Leakage Through an Open Wellbore from the Reservoir due to Carbon Dioxide Injection. https://escholarship.org/uc/item/49n090zc

Pan, L., C. M. Oldenburg, Y. Wu and K. Pruess, 2011a. T2Well/ECO2N Version 1.0: Multiphase and Non-Isothermal Model for Coupled Wellbore-Reservoir Flow of Carbon Dioxide and Variable Salinity Water, Report LBNL-4291E, Lawrence Berkeley National Laboratory, Berkeley, Calif..

Pan, L., Oldenburg, C.M., Freifeld, B.M. and Jordan, P.D., 2018a. Modeling the Aliso Canyon underground gas storage well blowout and kill operations using the coupled well-reservoir simulator T2Well. Journal of Petroleum Science and Engineering, 161, pp.158-174.

Pan, L., Oldenburg, C.M., and Zhou Q., 2018b. Improving convergence of ECO2M: Application to three-phase systems with liquid-gas phase change. TOUGH SYMPOSIUM 2018, Berkeley, CA 94720, USA, October 8-10, 2018.

Pan, L., Spycher, N., Doughty, C. and Pruess, K., 2017. ECO2N V2. 0: A TOUGH2 fluid property module for modeling CO_2-H_2O-NACL systems to elevated temperatures of up to 300° C. Greenhouse Gases: Science and Technology, 7(2), pp.313-327.

Pawar, R.J., Bromhal, G.S., Chu, S., Dilmore, R.M., Oldenburg, C.M., Stauffer, P.H., Zhang, Y. and Guthrie, G.D., 2016. The National Risk Assessment Partnership's integrated assessment model for carbon storage: A tool to support decision making amidst uncertainty. International Journal of Greenhouse Gas Control, 52, pp.175-189.

Pruess, K., 2003. Numerical simulation of CO_2 leakage from a geologic disposal reservoir including transitions from super-to sub-critical conditions, and boiling of liquid of CO_2. Society of Petroleum Engineering Journal, 9(2), pp.237-248.

Pruess, K. and Spycher, N., 2007. ECO2N–A fluid property module for the TOUGH2 code for studies of CO_2 storage in saline aquifers. *Energy Conversion and Management*, *48*(6), pp.1761-1767.

Pruess, K., 2011. ECO_2M: a TOUGH2 fluid property module for mixtures of water, NaCl, and CO_2, including super-and sub-critical conditions, and phase change between liquid and gaseous CO_2.

Pruess, K., C. Oldenburg, and G. Moridis, *TOUGH2 User's Guide, Version 2.1*, Report LBNL-43134, Lawrence Berkeley National Laboratory, Berkeley, Calif., 2012.

Tao, Q., Checkai, D., Huerta, N.J. and Bryant, S.L., 2010, January. Model to predict CO2 leakage rates along a wellbore. In *SPE annual technical conference and exhibition*. Society of Petroleum Engineers.

Wojtanowicz, A.K., Nishikawa, S. and Rong, X., 2001. Diagnosis and remediation of sustained casing pressure in wells. Final Report. Louisiana State University, Virginia. Submitted to: US Department of Interior, Minerals Management Service.

Xu, R. and Wojtanowicz, A.K., 2001, January. Diagnosis of sustained casing pressure from bleed-off/buildup testing patterns. In SPE Production and Operations Symposium. Society of Petroleum Engineers.